Supplemental Material for Density-Corrected Density Functional Theory for Solids

Youngsam Kim[a], Suhwan Song[a†], Mihira Sogal[b], Kieron Burke[b,c], and Eunji Sim[a*]

[a]Department of Chemistry, Yonsei University, 50 Yonsei-ro Seodaemun-gu, Seoul 03722, Korea.

[b]Department of Chemistry, University of California, Irvine, CA 92697, USA.

[c]Department of Physics and Astronomy, University of California, Irvine, CA 92697, USA.

Contents

[†]Present address: Vertical AI2 Team, AI Center, Samsung Electronics, 130 Samsung-ro, Suwon, 16678, Korea

[*]esim@yonsei.ac.kr

S1. Computational Details

All DFT calculations were performed using FHI-aims [1] (version 230214). Molecular crystals and CO/NaCl(100) adsorption system were treated with the NAO-VCC-nZ basis sets (n = 3, 4) to approach the complete-basis-set (CBS) limit. [2] The CBS energy was obtained by two-point extrapolation between the NAO-VCC-3Z and -4Z levels:

$$E[\infty] = \frac{E[n_1]n_1^3 - E[n_2]n_2^3}{n_1^3 - n_2^3} \tag{S1}$$

where $E[n]$ is the total energy for the NAO-VCC-nZ basis sets. The basis-set quality was validated against plane-wave results from Ref. 3, showing good agreement (Fig. S1 (a) and (b)). For covalent solids and graphite, the *tight* setting with a default basis set tier was employed due to the hard convergence of NAO-VCC-nZ.

Brillouin zones were sampled using Γ-centered k-point meshes: 9 × 9 × 9 for dia-Si, 3C-SiC, and 8 × 8 × 8 for dia-C, 3 × 3 × 3 for ice phases, 3 × 6 × 1 for surface adsorption system, 8 × 8 × 2 for graphite, and 8 × 8 × 1 for graphene. For X23, standard k-point mesh was used. [4] Structures for the ice phases from Ref. 5 with r^{2}SCAN-3c optimized structures, and those for the X23 from Ref. 6. The water monomer was optimized at the CCSD(T)/aug-cc-pV5Z level using PySCF [7].

In HF-DFT calculation, the HF density is fixed and no more self-consistent loop should be performed. The total energy is obtained by evaluating the exchange-correlation energy on the fixed HF density, replacing the exact-exchange term, while all other energy components remain those of the HF calculation. The *xc* and *total_energy_method* tags in *control.in* file were set to Hartree-Fock (hf) and the chosen exchange-correlation functional, respectively, for the HF-DFT calculations in FHI-aims. The self-consistent PBE, HF, and non-self-consistent HF-PBE dissociation curves for NaCl are shown in Fig. S1 (c). The energy components at a 2.4 Å bond distance are compared in Tables S1.

For dispersion corrections, we utilize DFT-D4 [8] method. In this approach, the dispersion energy (E^{D4}) is explicitly added to self-consistent DFT total energy and is given by,

$$E^{\mathrm{D4}} = \underbrace{-\sum_{AB}\sum_{n}^{6,8} s_n \frac{C_n^{AB}}{R_{AB}^n} f_{\mathrm{damp}}^n(R_{AB})}_{E^{(2)}} + E^{(3)} \tag{S2}$$

where the summations run over all atom pairs A and B separated by a distance R_{AB}. The damping functions (f_{damp}^n) prevent divergence at short range and is expressed as,

$$f_{\mathrm{damp}}^n(R_{AB}) = \frac{1}{1 + (R_1^{AB}/R_{AB})^n} \tag{S3}$$

where $R_1^{AB} = a_1 R_0^{AB} + a_2$ is a scaled and shifted van der Waals radius R_0^{AB}, and a_1 and a_2 are global parameters optimized for each density functional. The s_8, a_1, and a_2 parameters for D^{2}C-DFT were refitted using HF-DFT energies for density-insensitive systems, ensuring that dispersion correction term cures only the residual functional error. [9] The parameters utilized are shown in Table S2.

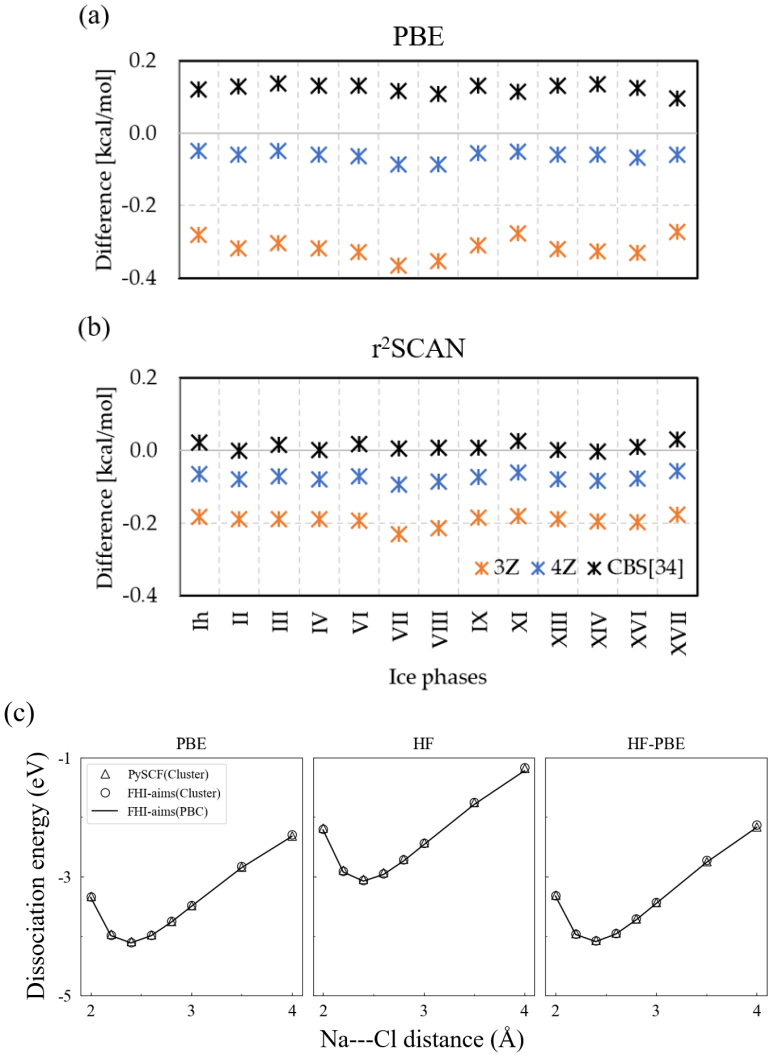

Figure S1: Validation between different codes. (a) and (b) show comparison of 13 ice phases cohesive energies between VASP [10] and FHI-aims [1] results. VASP results are taken from Ref. 3, where hard pseudopotentials with 1000 eV cutoff and a dense FFT grid are used. (c) Dissociation curves for NaCl. Cluster calculations from PySCF (FHI-aims) are shown as triangles (circles) without lines, while periodic results from FHI-aims are plotted as solid lines without markers. For periodic calculations, the unit cell is defined as a cubic box of 20Å×21Å×22Å.

Table S1: NaCl calculations at a bond distance of 2.4 Å using both cluster and periodic boundary condition (PBC) approaches. PySCF and FHI-aims calculations employ the def2-QZVPPD and NAO-VCC-4Z basis sets, respectively. Here, HF-DFT is denoted as PBE[HF]. Kinetic energy (E_T), Coulomb interactions (nuclear-electron E_{ne}, electron-electron E_J, nuclear-nuclear E_{nn}), exchange-correlation energy (E_{xc}), and the total energy (E_{tot}) are shown in Hartree. Note that for periodic calculations, the unit cell for Na and Cl atoms is defined as a cubic box of 20Å×21Å×22Å.

Cluster PySCF	E_T	E_{ne}	E_J	E_{nn}	E_{xc}	E_{tot}
PBE	620.82	-1568.18	326.26	41.23	-42.42	-622.29
HF	621.46	-1569.25	326.79	41.23	-41.69	-621.46
PBE[HF]	621.46	-1569.25	326.79	41.23	-42.51	-622.28
Diff. (HF - PBE[HF])	0.00	0.00	0.00	0.00	0.82	0.82
Cluster FHI-aims	E_T	E_{ne}+E_J+E_{nn}			E_{xc}	E_{tot}
PBE	621.38	-1201.23			-42.44	-622.30
HF	621.46	-1201.22			-41.69	-621.46
PBE[HF]	621.46	-1201.22			-42.51	-622.28
Diff. (HF - PBE[HF])	0.00	0.00			0.81	0.81
PBC FHI-aims	E_T	E_{ne}+E_J+E_{nn}			E_{xc}	E_{tot}
PBE	621.38	-1201.23			-42.44	-622.30
HF	621.46	-1201.22			-41.69	-621.46
PBE[HF]	621.46	-1201.22			-42.51	-622.28
Diff. (HF - PBE[HF])	0.00	0.00			0.81	0.81

Table S2: D4 parameters used in this work. s_6 is set to 1. D4 calculations were performed using *dftd4* version 3.4.0. (*https://github.com/dftd4/dftd4*)

	D^2C-DFT			DFT-D4			
	s_8	a_1	a_2	s_8	a_1	a_2	Ref
PBE	1.78595387	0.88511469	2.32863362	0.95948085	0.38574991	4.80688534	11
PBEsol	N/A			1.71885698	0.47901421	5.96771589	**?**
r^2SCAN	0.02734375	0.474707031	3.34667969	0.60187490	0.51559235	5.77342911	12

S2. Density Dependence of Cohesive Energies

Table S3: Errors in cohesive energy ΔE_{coh} (in eV/atom) for dia-C, dia-Si, and 3C-SiC. The rows represent different exchange-correlation (XC) functionals, while the columns indicate the density used in a non-self-consistent manner. No dispersion corrections are included. Self-consistent results are highlighted in yellow; the last column ($\tilde{S}$) reports the energy difference between evaluations on HF and LDA densities. Reference E_{coh} (eV/atom):[13] C-7.55, Si-4.68, SiC-6.48.

ΔE_{coh}(eV/atom)		Density				
dia-C		PZ-LDA	PBE	r^{2}SCAN	HF	$\tilde{S}$
XC	PZ-LDA	1.460	1.410	1.361	1.194	0.267
	PBE	0.188	0.186	0.221	0.072	0.116
	r^{2}SCAN	-0.028	-0.026	0.013	-0.108	0.080
dia-Si		PZ-LDA	PBE	r^{2}SCAN	HF	Var.
XC	PZ-LDA	0.698	0.666	0.648	0.406	0.293
	PBE	-0.024	-0.083	-0.070	-0.269	0.245
	r^{2}SCAN	0.250	0.032	0.069	-0.089	0.340
3C-SiC		PZ-LDA	PBE	r^{2}SCAN	HF	Var.
XC	PZ-LDA	0.995	0.957	0.911	0.695	0.301
	PBE	-0.014	-0.046	-0.028	-0.207	0.193
	r^{2}SCAN	0.095	-0.012	0.034	-0.088	0.183

S3. Equation of state fits for Covalent Solids

For covalent solids, the cohesive energy $E_{\mathrm{coh}}(=-E_0)$, equilibrium volume V_0, and bulk modulus B_0 were determined through the fitting of cohesive energies along the various lattice constants a_0 within a range of $V_0 \pm 20\%$ to a third-order Birch-Murnaghan equation of state (EOS)[14] as follows:

$$E(V) = E_0 + \frac{9V_0B_0}{16}\left\{\left[\left(\frac{V_0}{V}\right)^{\frac{2}{3}} - 1\right]^3 B_0' + \left[\left(\frac{V_0}{V}\right)^{\frac{2}{3}} - 1\right]^2 \left[6 - 4\left(\frac{V_0}{V}\right)^{\frac{2}{3}}\right]\right\} \tag{S4}$$

where B_0' is the pressure derivative of the bulk modulus. The raw data used for fitting are given in Supplemental Material.

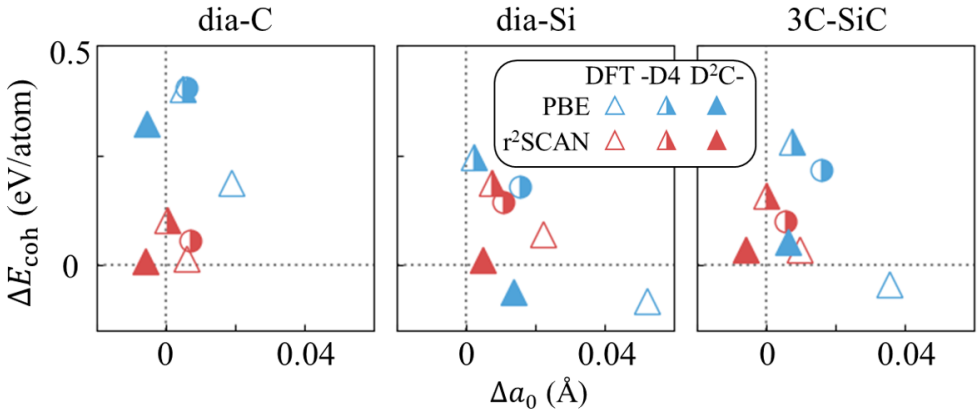

Figure S2: Errors in cohesive energy (ΔE_{coh}) and lattice constant (Δa_0). Half-filled blue circle denote PBE+MBD@rsSCS results and half-filled red circles denote r^{2}SCAN+rVV10 results.

Table S4: Deviations relative to experimental values[13] in cohesive energy E_{coh}, lattice constant a_0, and bulk modulus B_0 for dia-C, 3C-SiC, and dia-Si.

		ΔE_{coh}	Δa_0	ΔB_0
		% (eV/atom)	% (pm)	% (GPa)
PBE	dia-C	2.5 (0.19)	0.5 (1.9)	-4.7 (-21.6)
	3C-SiC	-0.7 (-0.05)	0.8 (3.6)	-7.5 (-17.2)
	dia-Si	-1.9 (-0.09)	1.0 (5.2)	-11.8 (-11.8)
PBE-D4	dia-C	5.4 (0.40)	0.1 (0.5)	-2.6 (-11.8)
	3C-SiC	4.3 (0.28)	0.2 (0.8)	-4.8 (-11.1)
	dia-Si	5.1 (0.24)	0.0 (0.2)	-10.6 (-10.7)
PBE+MBD@rsSCS	dia-C	5.4 (0.40)	0.2 (0.6)	-2.8 (-12.7)
	3C-SiC	3.3 (0.22)	0.4 (1.6)	-4.1 (-9.4)
	dia-Si	3.8 (0.18)	0.3 (1.5)	-7.3 (-7.4)
HF-PBE	dia-C	1.0 (0.08)	0.3 (1.2)	-2.3 (10.4)
	3C-SiC	2.8 (-0.18)	0.6 (2.8)	-4.6 (10.6)
	dia-Si	-5.8 (-0.27)	0.8 (4.1)	-8.3 (-8.4)
D^2C-PBE	dia-C	4.3 (0.33)	-0.2 (-0.5)	0.2 (0.9)
	3C-SiC	1.2 (0.08)	0.1 (0.6)	-2.8 (-6.3)
	dia-Si	-1.4 (-0.07)	0.3 (1.4)	-8.7 (-8.8)
r^2SCAN	dia-C	0.3 (0.02)	0.2 (0.6)	-0.5 (-2.4)
	3C-SiC	-0.4 (-0.02)	0.2 (1.0)	-0.5 (-1.2)
	dia-Si	1.4 (0.06)	0.4 (2.2)	-3.2 (-3.2)
r^2SCAN-D4	dia-C	1.4 (0.11)	0.0 (0.0)	0.4 (1.9)
	3C-SiC	1.5 (0.10)	0.0 (0.0)	0.4 (1.0)
	dia-Si	3.9 (0.18)	0.1 (0.7)	-3.3 (-3.3)
r^2SCAN+rVV10	dia-C	0.7 (0.55)	0.2 (0.7)	-0.6 (-2.9)
	3C-SiC	1.5 (0.10)	0.1 (0.5)	-0.3 (-0.8)
	dia-Si	3.1 (0.14)	0.2 (1.1)	-2.3 (-2.4)
HF-r^2SCAN	dia-C	-1.4 (-0.10)	0.0 (0.1)	1.3 (6.1)
	3C-SiC	-1.8 (-0.11)	0.1 (0.3)	2.2 (5.1)
	dia-Si	-2.0 (-0.09)	0.3 (1.7)	-0.9 (-0.9)
D^2C-r^2SCAN	dia-C	0.2 (0.01)	-0.2 (-0.6)	2.6 (11.7)
	3C-SiC	0.1 (0.01)	-0.1 (-0.6)	3.1 (7.1)
	dia-Si	0.1 (0.01)	0.1 (0.5)	-0.9 (-0.9)
PBEsol	dia-C	9.9 (0.75)	0.0 (0.2)	-1.2 (-5.2)
	3C-SiC	6.5 (0.42)	0.3 (1.2)	-3.6 (-8.3)
	dia-Si	6.2 (0.29)	0.3 (1.7)	-7.2 (-7.3)
PBEsol-D4	dia-C	11.5 (0.87)	-0.2 (-0.7)	0.1 (0.6)
	3C-SiC	9.4 (0.61)	-0.1 (-0.4)	-2.1 (-4.8)
	dia-Si	10.2 (0.48)	-0.2 (-0.9)	-7.1 (-7.1)
Exp.[†]	dia-C	7.55	355.3	454.7
	3C-SiC	6.48	434.6	229.1
	dia-Si	4.68	542.1	100.8

S4. Equation of state fits analysis

Lejaeghere *et al.*[15] suggested a gauge (Δ_{gauge}) that can quantify the difference between the fitted EoS curves as follows:

$$\Delta_{\text{gauge}}(a,b) = \sqrt{\frac{\int_{V_1}^{V_2}(E^a(V) - E^b(V))^2\,dV}{V_2 - V_1}}. \tag{S5}$$

The authors utilized $V_0 \pm 6\%$ ($V_1 = 0.94V_0$ and $V_2 = 1.06V_0$) for fitting the EoS curve and we chose $V_0 \pm 20\%$[16]. For brevity, Δ_{gauge}(DFT, reference) with $V_0 \pm 20\%$ is hereafter denoted as Δ_{gauge}. By subtracting the absolute error of cohesive energy ($\Delta E_{\text{coh}} = E_{\text{coh}}^{\text{DFT}} - E_{\text{coh}}^{\text{REF}}$) from Δ_{gauge}, we can extract the higher-order contributions, including B_0, to the difference in the curve.

Table S5: Comparison of Δ_{gauge}, ΔE_{coh}, and $\%\Delta B_0$ ($\frac{B_0^{\text{DFT}} - B_0^{\text{REF}}}{B_0^{\text{REF}}} \times 100\%$) across different functionals for three covalent solids. Note that the units are meV/atom except for $\%\Delta B_0$ (in %).

	PBE	PBE-D4	HF-PBE	D^{2}C-PBE	r^{2}SCAN	r^{2}SCAN-D4	HF-r^{2}SCAN	D^{2}C-r^{2}SCAN
				Dia-C				
Δ_{gauge}	185.7	401.1	72.5	323.8	16.1	102.8	109.4	10.9
ΔE_{coh}	-186.5	-399.9	-72.3	-322.3	-14.4	-103.3	107.6	-6.8
$\Delta_{\text{gauge}} - \lvert\Delta E_{\text{coh}}\rvert$	-0.8	1.2	0.2	1.5	1.7	-0.6	1.8	4.1
$\%\Delta B_0$	-5	-3	-2	0	-1	0	1	3
				Dia-Si				
Δ_{gauge}	94.3	253.0	273.4	57.5	69.3	189.2	92.7	11.7
ΔE_{coh}	82.9	-244.7	268.6	60.9	-69.4	-187.8	89.2	-11.3
$\Delta_{\text{gauge}} - \lvert\Delta E_{\text{coh}}\rvert$	11.4	8.3	4.8	-3.5	0.0	1.5	3.5	0.4
$\%\Delta B_0$	-12	-11	-8	-9	-3	-3	-1	-1
				3C-SiC				
Δ_{gauge}	67.6	281.5	191.9	76.9	31.5	96.1	119.5	7.5
ΔE_{coh}	48.6	-278.8	184.2	-75.6	26.8	-96.6	116.5	-5.1
$\Delta_{\text{gauge}} - \lvert\Delta E_{\text{coh}}\rvert$	19.0	2.7	7.7	1.3	4.7	-0.5	3.0	2.4
$\%\Delta B_0$	-7	-5	-5	-3	-1	0	2	3

S5. X23 Benchmark Using DMC Reference

Table S6: Mean error (ME) and mean absolute error (MAE) in cohesive energies (kcal/mol) for the X23 dataset using diffusion Monte Carlo (DMC) references.[17]. The dataset is grouped into hydrogen-bond (H-bond), mixed (Mix), and van der Waals (vdW) categories, with system counts in parentheses. The lowest MAE in each category is in bold.

		X23 (23)			H-bond (8)			Mix (4)			vdW (11)		
(kcal/mol)		DFT	-D4	D²C-	DFT	-D4	D²C-	DFT	-D4	D²C-	DFT	-D4	D²C-
PBE	ME	11.6	0.0	-1.0	8.5	0.0	0.1	11.4	-0.5	-1.3	13.8	0.2	-1.7
	MAE	11.6	**0.6**	1.3	8.5	0.8	**0.7**	11.4	**0.5**	1.3	13.8	**0.5**	1.7
r²SCAN	ME	5.9	-0.4	0.1	3.5	-0.7	0.3	5.7	-0.6	0.1	7.6	-0.1	-0.1
	MAE	5.9	**0.6**	0.7	3.5	0.7	**0.5**	5.7	0.6	**0.1**	7.6	**0.4**	1.1

S6. Graphite interlayer binding

The binding energy $E_{\mathrm{bind}}(z)$ as a function of interlayer separation z is defined as

$$E_{\mathrm{bind}}(z) = \frac{1}{4}E_{\mathrm{graphite}}(z) - \frac{1}{2}E_{\mathrm{graphene}} \tag{S6}$$

where $E_{\mathrm{graphite}}(z)$ and E_{graphene} are the total energies per unit cell of bulk graphite and graphene, respectively, and the prefactors ensure that E_{bind} is expressed per atom.

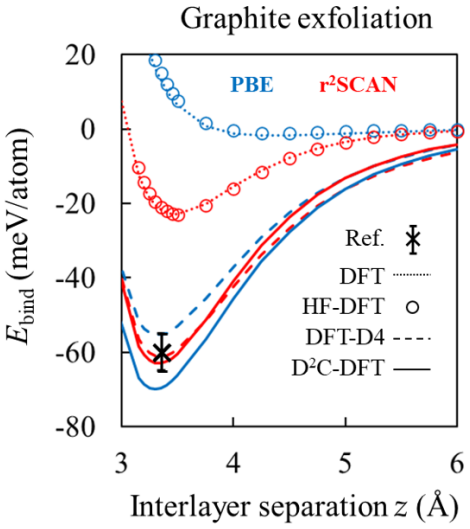

Figure S3: Interlayer binding energy of graphite as a function of interlayer separation. DMC value as the reference is taken from Ref. 18. Data given in Supplemental Material.

S7. Dispersion and Density Effects in and Covalent Solids and Graphite

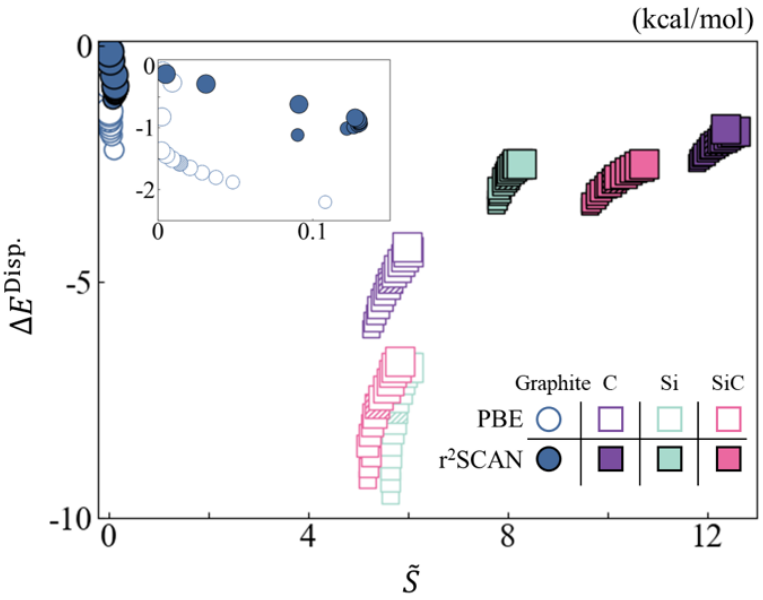

Figure S4: Comparison of dispersion correction ($\Delta E^{\text{Disp.}} = E^{\text{DFT-D4}} - E^{\text{DFT}}$) and density sensitivity ($\tilde{S}$) for graphite binding energies and $-E_{\text{coh}}$ of covalent solids. Note that cohesive energies are plotted with a negative sign for consistency with graphite binding energies. The marker size indicates interlayer separation for graphite or lattice constant for covalent solids, and hatched markers indicate equilibrium. The interlayer separation in graphite exfoliation ranges from 2.95 to 6 Å. The inset highlights the graphite results.

References

(1) Blum, V.; Gehrke, R.; Hanke, F.; Havu, P.; Havu, V.; Ren, X.; Reuter, K.; Scheffler, M. Ab initio molecular simulations with numeric atom-centered orbitals. *Comput. Phys. Commun.* **2009**, *180*, 2175–2196.

(2) Zhang, I. Y.; Ren, X.; Rinke, P.; Blum, V.; Scheffler, M. Numeric atom-centered-orbital basis sets with valence-correlation consistency from H to Ar. *New J. Phys.* **2013**, *15*, 123033.

(3) Della Pia, F.; Zen, A.; Alfè, D.; Michaelides, A. DMC-ICE13: Ambient and High Pressure Polymorphs of Ice From Diffusion Monte Carlo and Density Functional Theory. *J. Chem. Phys.* **2022**, *157*.

(4) Loboda, O. A.; Dolgonos, G. A.; Boese, A. D. Towards hybrid density functional calculations of molecular crystals via fragment-based methods. *J. Chem. Phys.* **2018**, *149*.

(5) Grimme, S.; Hansen, A.; Ehlert, S.; Mewes, J.-M. r2SCAN-3c: A "Swiss army knife" composite electronic-structure method. *J. Chem. Phys.* **2021**, *154*.

(6) Reilly, A. M.; Tkatchenko, A. Understanding the role of vibrations, exact exchange, and many-body van der Waals interactions in the cohesive properties of molecular crystals. *J. Chem. Phys.* **2013**, *139*.

(7) Sun, Q.; Zhang, X.; Banerjee, S.; Bao, P.; Barbry, M.; Blunt, N. S.; Bogdanov, N. A.; Booth, G. H.; Chen, J.; Cui, Z.-H.; others Recent developments in the PySCF program package. *J. Chem. Phys.* **2020**, *153*.

(8) Caldeweyher, E.; Mewes, J.-M.; Ehlert, S.; Grimme, S. Extension and evaluation of the D4 London-dispersion model for periodic systems. *Phys. Chem. Chem. Phys.* **2020**, *22*, 8499–8512.

(9) Lee, M.; Kim, B.; Sim, M.; Sogal, M.; Kim, Y.; Yu, H.; Burke, K.; Sim, E. Correcting dispersion corrections with density-corrected DFT. *J. Chem. Theory Comput.* **2024**, *20*, 7155–7167.

(10) Kresse, G.; Furthmüller, J. Efficient Iterative Schemes for ab Initio Total-Energy Calculations Using a Plane-Wave Basis Set. *Phys. Rev. B* **1996**, *54*, 11169–11186.

(11) Caldeweyher, E.; Ehlert, S.; Hansen, A.; Neugebauer, H.; Spicher, S.; Bannwarth, C.; Grimme, S. A generally applicable atomic-charge dependent London dispersion correction. *J. Chem. Phys.* **2019**, *150*.

(12) Ehlert, S.; Huniar, U.; Ning, J.; Furness, J. W.; Sun, J.; Kaplan, A. D.; Perdew, J. P.; Brandenburg, J. G. r2SCAN-D4: Dispersion corrected meta-generalized gradient approximation for general chemical applications. *J. Chem. Phys* **2021**, *154*.

(13) Schimka, L.; Harl, J.; Kresse, G. Improved hybrid functional for solids: The HSEsol functional. *J. Chem. Phys.* **2011**, *134*.

(14) Birch, F. Finite elastic strain of cubic crystals. *Phys. Rev.* **1947**, *71*, 809.

(15) Lejaeghere, K.; Van Speybroeck, V.; Van Oost, G.; Cottenier, S. Error estimates for solid-state density-functional theory predictions: an overview by means of the ground-state elemental crystals. *Crit. Rev. Solid State Mater. Sci.* **2014**, *39*, 1–24.

(16) Zhang, G.-X.; Reilly, A. M.; Tkatchenko, A.; Scheffler, M. Performance of various density-functional approximations for cohesive properties of 64 bulk solids. *New J. Phys.* **2018**, *20*, 063020.

(17) Della Pia, F.; Zen, A.; Alfè, D.; Michaelides, A. How Accurate Are Simulations and Experiments for the Lattice Energies of Molecular Crystals? *Phys. Rev. Lett.* **2024**, *133*, 046401.

(18) Spanu, L.; Sorella, S.; Galli, G. Nature and strength of interlayer binding in graphite. *Phys. Rev. Lett.* **2009**, *103*, 196401.